The pull-off test for viscoelastic soft solids

Problem presented by

Guoping Lian
Unilever

Problem statement

An Atomic Force Microscope (AFM) can be used to plot force against separation when a sphere is pushed into a viscoelastic mucus layer on a soft plane substrate and then retracted. Unilever wish to have a mathematical model of the process that could be used to determine the viscoelastic properties of the mucus from the measurements. The Study Group developed such a model and showed that it could provide force-separation curves with the same qualitative features as those obtained by Unilever in their experiments.

Study Group contributors

David Allwright (Smith Institute)
Leah Band (University of Nottingham)
Maurice Blount (DAMTP)
Sunny Chui-Webster (DAMTP)
Linda Cummings (University of Nottingham)
Rosemary Dyson (OCIAM)
Ian Griffiths (OCIAM)
Oliver Jensen (University of Nottingham)
John King (University of Nottingham)
James Oliver (University of Nottingham)
David Parker (University of Edinburgh)
Sylvain Reboux (University of Nottingham)
Michele Taroni (OCIAM)
Dominic Vella (DAMTP)
Robert Whittaker (University of Nottingham)
Maxim Zyskin (Oxford)

Report prepared by

Sunny Chiu-Webster (University of Nottingham)
Rosemary Dyson (OCIAM)
David Parker (University of Edinburgh)
Dominic Vella (DAMTP)
Robert Whittaker (University of Nottingham)

1 Introduction

The adhesive interactions between adhesive soft solids covered with viscoelastic film are crucial for a number of problems related to biological systems like cell adhesion and mucoadhesion. The mucoadhesive interactions are of particular interest to Unilever since most Unilever products interact with mucosa substrates in some way. Foods and beverages interact with oral mucosa including salivary films; this interaction influences taste, mouthfeel and flavour release. Further down the gastrointestinal tract mucoadhesive interactions condition nutrition uptake and to a certain extent enable food digestion. In oral care products mucoadhesion is an important aspect of products' functionality.

Generally mucoadhesion can be described as an interaction of solid or semisolid particles or even liquid droplets with a mucosa substrate that can be defined as a "thick" (about 0.1–200 μm) proteinaceous film. Such adhesive interaction is different from the interaction with solid surfaces, even soft ones. The complexity stems form the fact that several contributions can be identified within the adhesive contact or during rupture of such an adhesive contact, including

(1) the adhesive force;

(2) the extension of the viscoelastic film that leads to the formation of one or several filaments and their subsequent necking failure;

(3) interfacial tension effects (usually small due to low interfacial energy between two water-based phases, *e.g.* bound and unbound layers) that lead to a capillary effect;

(4) the viscoelastic deformation of the substrates and soft bodies.

1.1 Motivation for theoretical analysis

In many instances it is required to perform an in-vitro assessment of the mucoadhesive properties of materials that are subject to a screening assay. One of the screening methods is a pull-off test using the AFM. The result of the test is a graph of force against indentation and separation. In the experiment one can vary the speeds of approach and retraction, applied load, dwell time, geometry of interacting surfaces, solvent *etc.*

The graph of force against separation combines all the effects listed above and does not allow the direct extraction of the parameters of interest, *e.g.* the extensional viscosity of the proteinaceous mucosa layer or the thickness of this layer. Even the adhesive energy between the mucosa itself and the probe is not measured directly. Since pull-off measurements are dynamic, the whole process can be described using differential equations, some of which are non-linear.

Therefore from Unilever's point of view the main purpose of the theoretical analysis is to establish a method for extracting the parameters of interest from fitting and modelling of an experimental force-separation curve, provided that the theoretical model is adequate

for the given experimental conditions. In addition, the theoretical model could provide some physical insights into which contributions are dominating the interaction.

Unilever hopes that the theoretical analysis of a force curve should provide following information:

- adhesive energy (for each of the interfaces — substrate1/film1, film1/film2, film2/substrate2);
- elastic parameters of the viscoelastic substrate;
- viscoelastic parameters of a thin polymer or proteinaceous film adjacent to a viscoelastic substrate;
- thickness of this thin polymer or proteinaceous film.

Unilever's overall aim is to develop a single assay test for mucoadhesive interaction, without needing separate experiments to disentangle the various contributions.

1.2 Definition of the problem and experiment

Consider two cases; (i) a viscoelastic solid sphere interacting with a flat mucosa substrate; and (ii) an elastic solid sphere coated with a viscoelastic polymer layer of thickness d interacting with a mucosa substrate. Both cases are illustrated in Figure 1.

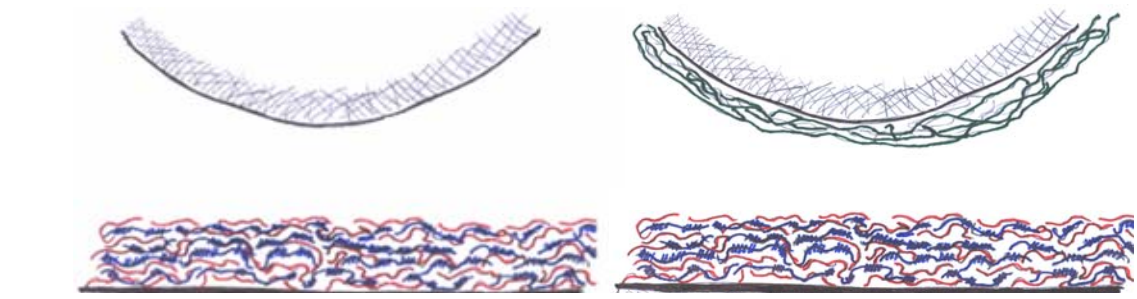

Figure 1: (i) a sphere interacting with a flat mucosa substrate; (ii) a sphere coated with a viscoelastic polymer of thickness d interacting with mucosa substrate.

The experiments conducted by Unilever suggest that the rupture of the adhesive coating happens in two stages. The first stage is hypothesised to be a rupture of a true adhesive contact, followed by a second stage that is due to the stretching of the polymer or proteinaceous filament. One has to consider also a number of physicochemical phenomena such as hydrodynamic drag, time-dependent adhesion, nonlinear load-dependent adhesion as well as capillary adhesion aggravated by elasto-capillary balance and necking failure. A schematic illustration of rupture, together with a corresponding force curve are presented in Figure 2.

The time-dependent contact adhesion effects are related to the dynamics of the polymer chains in the gap between the surfaces. The nonlinear load effects stem from the fact

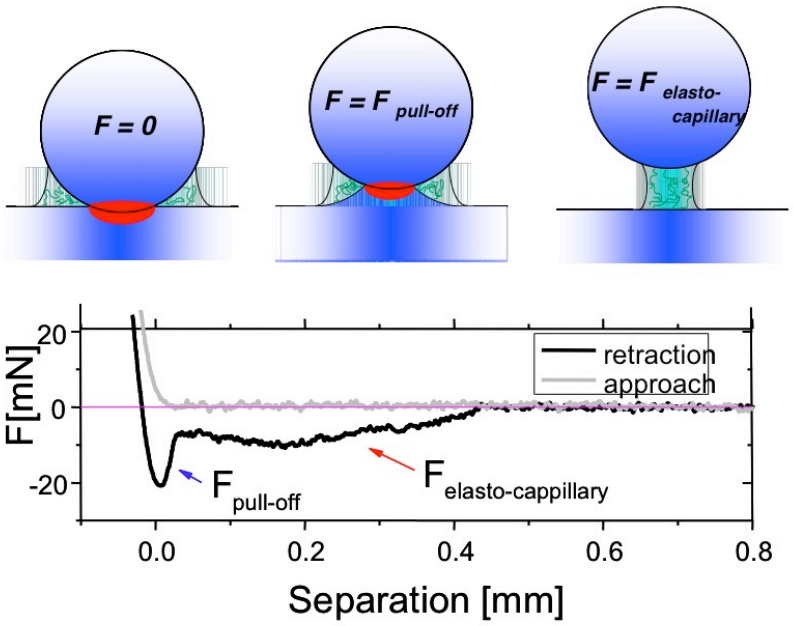

Figure 2: Force-separation curves during approach and retraction.

that the contact adhesive interaction can vary across the contact area following the non-uniform stress distribution; in this way polymer properties that are highly susceptible to the pressure or stress lead to a radial distribution in adhesive energy as well as a dependency on applied load. The elasto-capillary force arises from the extension of the viscoelastic polymer bridge that has been formed during the contact.

2 Outline description of experiment and model

The pull-off experiment is illustrated in Figure 3. The nominal separation between the base of the sphere and the substrate is

$$S = X - \Delta - 2R, \tag{1}$$

where X is the controlled distance of the substrate below the equilibrium position of the cantilever tip, Δ is the deflection of the cantilever tip, and $2R$ is the diameter of the sphere. The actual minimum separation h_0 between the bottom of the sphere and the substrate will be altered from the *nominal* separation S by the amount of any elastic compression of the sphere and substrate,

$$h_0 = S + \Delta_{\text{sph}} + \Delta_{\text{sub}}. \tag{2}$$

The cantilever is assumed linear so the upwards force exerted by the cantilever on the sphere is $F = k\Delta$. We shall mostly be considering the retraction phase, during which

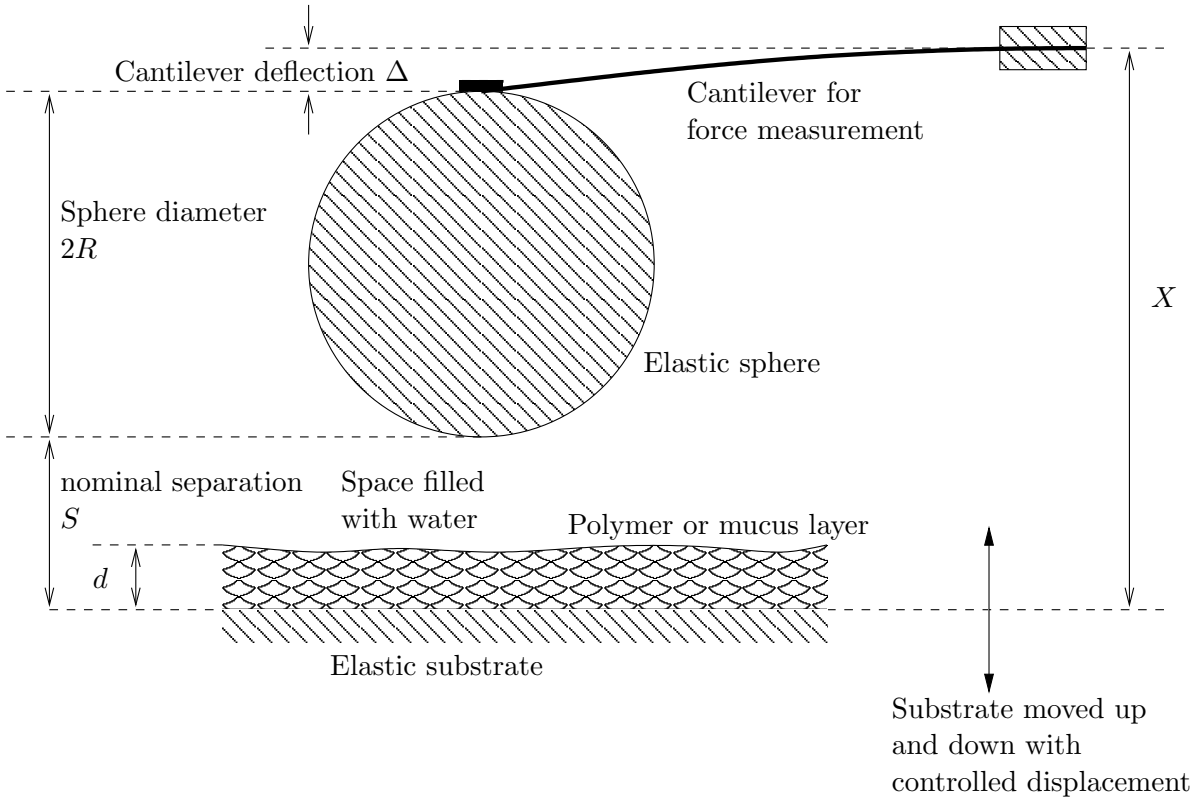

Figure 3: Schematic diagram of pull-off experiment.

$\Delta > 0$ and $F > 0$ so that the mucus layer is in tension. Note though that the force plotted by Unilever has the opposite sign to our F, so it is positive during the approach phase and negative during retraction. Although Unilever's question is about the inverse problem (given the force-separation curve, what are the material properties) we start with the forward problem of determining the curve if we knew the material parameters.

Figure 4 shows how the force-separation curve arises from the basic regimes of the experiment. During the approach phase, there is initially no force, until the sphere enters the mucus layer. Once it enters, the force is non-zero, and as the substrate is raised the cantilever deflects and the force increases. Then during the retraction phase, the sphere pulls some mucus off the substrate. There is initially a thin layer of mucus between the sphere and substrate, and a lubrication flow of mucus to fill the opening gap. Then as that gap opens wider, one or more filaments of mucus will link the sphere to the substrate. As the gap opens further still, those filaments will break and the force then returns to zero.

3 Mathematical models and assumptions

The forces acting on the sphere will arise from six causes, as illustrated in Figure 5:

(1) viscous drag on the sphere in the surrounding water,

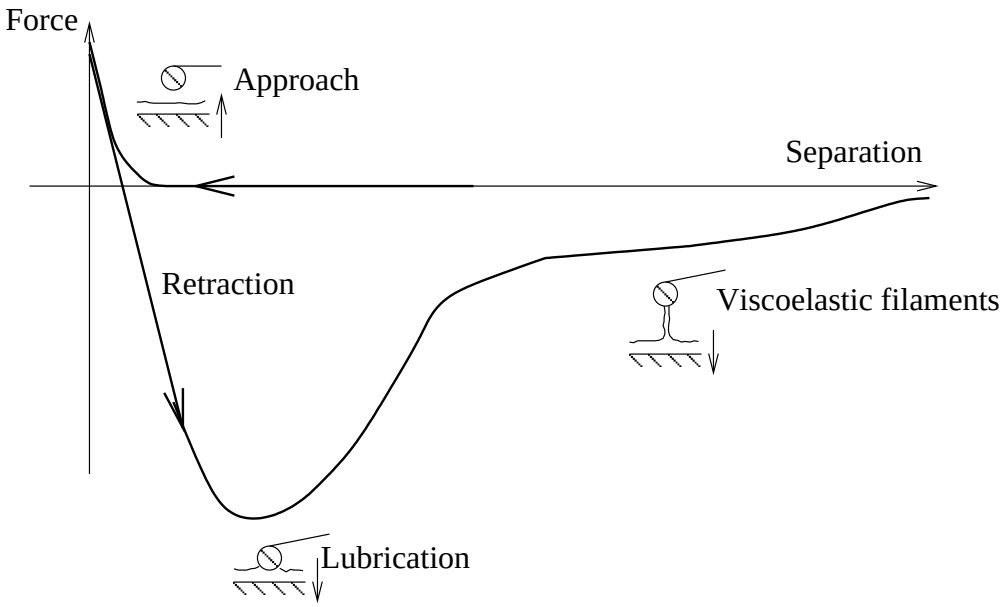

Figure 4: The different stages experiment corresponding to the different parts of the force-separation curve, in the case of no adhesion.

(2) the elastic force from the deflected cantilever,

(3) the viscoelastic squeeze film in the thin gap between the sphere and the base (which may perhaps be subject to cavitation),

(4) adhesion between the sphere and the base by electrostatic and van der Waals forces,

(5) elastic deformation of the sphere and base,

(6) the viscoelastic filament or filaments of material that are formed when the gap opens up.

The first of these, viscous drag in the water, turns out to be negligible when we estimate the Stokes drag $6\pi\mu RU$, and so it will be dropped from now on. The elastic force we model by a simple linearly elastic beam $F = k\Delta$. The viscoelastic squeeze film is discussed in Section 4. The adhesion forces were not analysed in detail but we comment on them in Section 7. The elastic forces give displacements Δ_{sph} and Δ_{sub} that are estimated to be small, so these were neglected. The viscoelastic filament is studied in Section 5.

When there is no adhesion, one natural lumped parameter model is to think of the force between the sphere and the base as the sum of one term from a lubrication layer and one from a filament. Modelling a lubrication layer with a nonlinear viscoelastic material leads to difficulties that are addressed in Appendix A but which have not been pushed through to a predictive equation yet. However, we do present the analysis for a Newtonian lubrication layer in Section 4.1, and for a *linearly* viscoelastic material in Section 4.2. Modelling a nonlinear viscoelastic filament is possible with the FENE-P model of nonlinear viscoelasticity, which is believed by Unilever to be a realistic

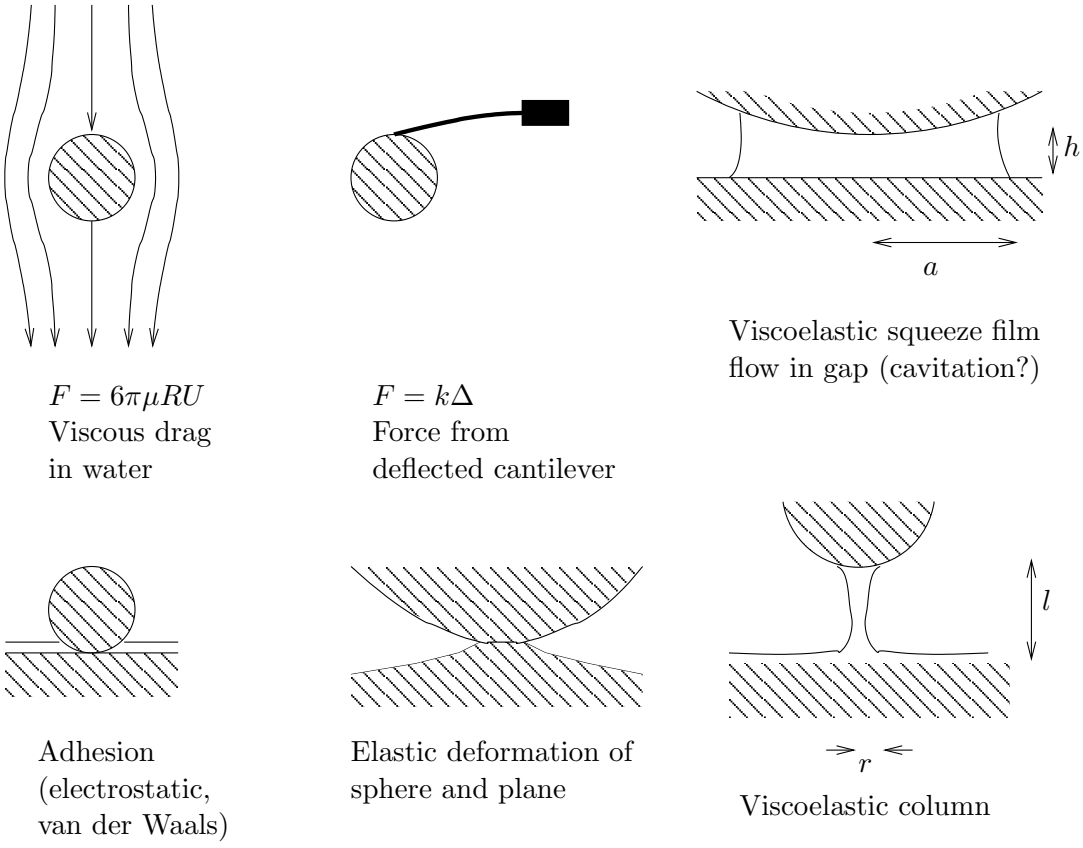

Figure 5: Forces on the sphere

representation of the properties of the mucus. This analysis is given in Section 5. The combination of these then gives results that are presented in Section 6. Finally, our conclusions and various issues where we made initial explorations but have not completed the analysis are summarized in Section 7.

4 Lubrication layer

The squeeze film can be modelled most simply by treating the fluid as Newtonian, and this is carried out in Section 4.1. Alternatively a viscoelastic model can be used and this is treated in Section 4.2.

4.1 Newtonian

We here calculate the force exerted when a rigid sphere of radius R is pulled off a rigid plane base covered with a layer of thickness d ($d \ll R$) of Newtonian fluid of viscosity μ. We shall let $h_0(t)$ denote the separation of the sphere from the plane, so that when h_0 is small we have the situation illustrated in Figure 6. When the sphere is initially pushed into the fluid film of thickness d, the radius of the wetted area of the sphere is of order

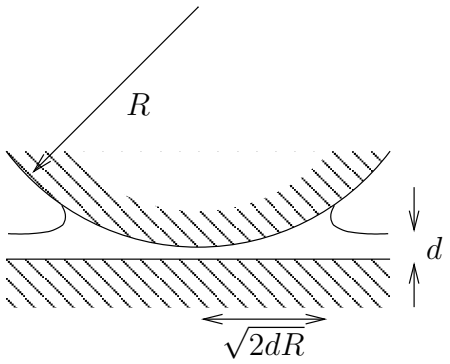

Figure 6: Viscous squeeze film before separation.

$a = \sqrt{2dR}$ and so the corresponding volume of fluid in the film is

$$V = \pi a^2 d = 2\pi d^2 R. \tag{3}$$

Part (about half) of this fluid is still contained in the gap between the sphere and the plane and the rest is pushed up into a collar around the contact roughly as illustrated. In the initial phase of separation illustrated on the left of Figure 7 when $h_0 \ll d$, the main forces come from a region with radius of order $\sqrt{2h_0R}$ and so the sphere can be approximated by a paraboloid and the squeeze film thickness at radius r from the vertical axis of symmetry is $h = h_0 + r^2/2R$. This approximation leads to the force required to

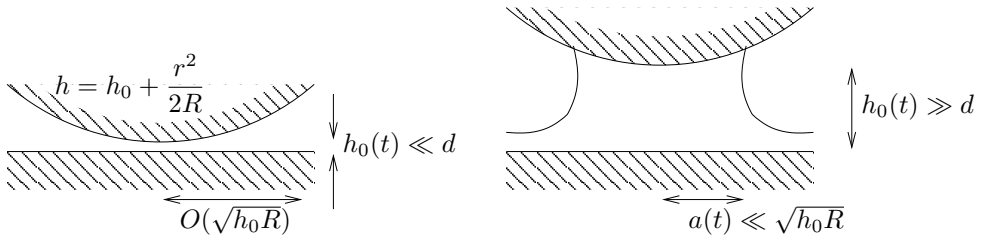

Figure 7: The spherical and planar regimes of the inverse squeeze film during separation.

separate the sphere from the plane being (in the lubrication approximation)

$$F_l = \frac{6\pi\mu\dot{h}_0 R^2}{h_0}. \tag{4}$$

Later in the separation, we enter the planar regime illustrated on the right of Figure 7 where we assume that the volume V of fluid forms an approximately cylindrical region. Applying the lubrication approximation again we obtain the force in the form

$$F_l = \frac{6\pi\mu\dot{h}_0 d^4 R^2}{4h_0^5}. \tag{5}$$

Combining (4) and (5) into a single equation that takes these forms when $h_0 \ll d$ and $h_0 \gg d$ respectively, we approximate the force by

$$F_l = \frac{6\pi\mu\dot{h}_0 R^2}{h_0}\left(\frac{d^4}{4h_0^4 + d^4}\right). \tag{6}$$

4.2 Viscoelastic squeeze film

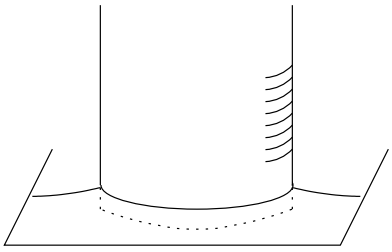

Figure 8: Circular cylinder pulled out of a viscoelastic squeeze film.

When the fluid is treated as a linear viscoelastic Maxwell fluid, rather than Newtonian, the force can be calculated for a circular cylinder pulled out of a fluid layer, to obtain the differential equation for gap width $h(t)$ corresponding to a given applied force $F(t)$. The situation is illustrated in Figure 8. The fluid model takes the form

$$\sigma + \mathrm{De}\,\dot{\sigma} = \dot{\gamma}, \tag{7}$$

where De is the Deborah number (defined in detail later). For $\mathrm{De} \ll 1$, one can do a perturbation analysis leading to a differential equation for film height $h(t)$, for the given pulling force $F(t)$:

$$F(t) = \frac{a\dot{h}}{h^3} - \mathrm{De}\left(\frac{\ddot{h}}{h^3} - \frac{33\dot{h}^2}{10h^4}\right) + O(\mathrm{De}^2). \tag{8}$$

For a constant force F, the separation h tends to infinity in finite time.

5 Nonlinear viscoelastic filament

We now derive the equations for a slender viscoelastic filament when the constitutive law for the material is the FENE-P model (finite extension nonlinear elasticity, with Peterlin's closure assumption). The governing equations are

- Conservation of mass:

$$\nabla \cdot \mathbf{u} = 0. \tag{9}$$

- Force balance (for slow flow):

$$-\nabla p + \nabla \cdot \boldsymbol{\tau}_{tot} = \mathbf{0}. \tag{10}$$

- FENE-P constitutive equations for the stress tensor:

$$\begin{aligned}
\boldsymbol{\tau}_{tot} &= \boldsymbol{\tau}_s + \boldsymbol{\tau}, && (11)\\
\boldsymbol{\tau}_s &= \eta_s \dot{\boldsymbol{\gamma}}, && (12)\\
F\boldsymbol{\tau} + \lambda \overset{\triangledown}{\boldsymbol{\tau}} - \frac{D}{Dt}\Big(\ln(F)\Big)\left(\lambda\boldsymbol{\tau} + \frac{b}{b+2}\eta_p \mathbf{I}\right) &= \frac{b}{b+2}\eta_p \dot{\boldsymbol{\gamma}}, && (13)\\
F &= 1 + \frac{3}{b}\left(1 + \frac{\lambda}{3\eta_p} Tr(\boldsymbol{\tau})\right), && (14)\\
\dot{\boldsymbol{\gamma}} &= \nabla\mathbf{u} + (\nabla\mathbf{u})^T. && (15)
\end{aligned}$$

In these equations, the four parameters are taken to have values given by Unilever:

$$\eta_p = 0.68\,\mathrm{Pa\,s}, \qquad \eta_s = 1.5\times10^{-3}\,\mathrm{Pa\,s}, \qquad \lambda = 252\,\mathrm{s}, \qquad b = 50. \tag{16}$$

We now wish to nondimensionalize these for extensional flow of a slender filament, so we let L be the filament length, ϵL its radius, and scale the quantities accordingly:

$$z = L\hat{z}, \quad r = \epsilon L\hat{r}, \quad \boldsymbol{u} = (u_r, u_\theta, u_z) = U(\epsilon\hat{u}, 0, \hat{w}), \quad t = \frac{L}{U}\hat{t}, \tag{17}$$

$$(p, \tau_{zz}, \tau_{rr}, \tau_{\theta\theta}, \tau_{rz}) = \frac{\eta_p U}{L}(\hat{p}, \hat{\tau}_{zz}, \hat{\tau}_{rr}, \hat{\tau}_{\theta\theta}, \epsilon\hat{\tau}_{rz}). \tag{18}$$

At leading order (and dropping the ˆs) we then have conservation of mass in the form

$$\frac{\partial u}{\partial r} + \frac{u}{r} + \frac{\partial w}{\partial z} = 0. \tag{19}$$

and the force balance

$$\frac{\partial p}{\partial r} = \frac{\partial \tau_{rr}}{\partial r} + \frac{\tau_{rr} - \tau_{\theta\theta}}{r} + \beta\left(\frac{1}{r}\frac{\partial}{\partial r}\left(r\frac{\partial u}{\partial r}\right) - \frac{u}{r^2}\right), \tag{20}$$

$$0 = \frac{\beta}{r}\frac{\partial}{\partial r}\left(r\frac{\partial w}{\partial r}\right), \tag{21}$$

and the constitutive equations

$$F\tau_{rr} + \mathrm{De}\left(\frac{D\tau_{rr}}{Dt} - 2\tau_{rr}\frac{\partial u}{\partial r}\right) = \left(\mathrm{De}\,\tau_{rr} + \alpha\right)\frac{D}{Dt}(\ln(F)) + 2\alpha\frac{\partial u}{\partial r}, \tag{22}$$

$$F\tau_{zz} + \mathrm{De}\left(\frac{D\tau_{zz}}{Dt} - 2\tau_{rz}\frac{\partial w}{\partial r} - 2\tau_{zz}\frac{\partial w}{\partial z}\right) = \left(\mathrm{De}\,\tau_{zz} + \alpha\right)\frac{D}{Dt}(\ln(F)) + 2\alpha\frac{\partial w}{\partial z}, \tag{23}$$

$$F\tau_{\theta\theta} + \mathrm{De}\left(\frac{D}{Dt}\tau_{\theta\theta} - 2\tau_{\theta\theta}\frac{u}{r}\right) = \left(\mathrm{De}\,\tau_{\theta\theta} + \alpha\right)\frac{D}{Dt}\big(\ln(F)\big) + 2\alpha\frac{u}{r}, \tag{24}$$

$$(\mathrm{De}\,\tau_{rr} + \alpha)\frac{\partial w}{\partial r} = 0, \tag{25}$$

where

$$F = 1 + \frac{3}{b}\left(1 + \frac{\mathrm{De}}{3}(2\tau_{rr} + \tau_{zz})\right). \tag{26}$$

In these equations, the Deborah number De and the two other dimensionless parameters are

$$\mathrm{De} = \frac{\lambda U}{L}, \quad \beta = \frac{\eta_s}{\eta_p}, \quad \alpha = \frac{b}{b+2}. \tag{27}$$

The usual kinematic and zero traction boundary conditions then give

$$\frac{\partial w}{\partial r} = 0, \quad u = -\frac{r}{2}\frac{\partial w}{\partial z}, \quad \tau_{rr} = \tau_{\theta\theta} = p. \tag{28}$$

Conservation of mass and force balance reduce to

$$(R^2)_t + (R^2 w)_z = 0, \tag{29}$$

$$R^2(\tau_{zz} - \tau_{rr}) + 3\beta R^2 \frac{\partial w}{\partial z} + \Gamma R = T(t), \tag{30}$$

where $T(t)$ is the tension in the filament (as in the Trouton model).

The constitutive laws become

$$F\tau_{zz} + \mathrm{De}\left(\frac{D\tau_{zz}}{Dt} - 2\tau_{zz}\frac{\partial w}{\partial z}\right) = (\mathrm{De}\,\tau_{zz} + \alpha)\frac{D}{Dt}(\ln(F)) + 2\alpha\frac{\partial w}{\partial z}, \tag{31}$$

$$F\tau_{rr} + \mathrm{De}\left(\frac{D\tau_{rr}}{Dt} + \tau_{rr}\frac{\partial w}{\partial z}\right) = (\mathrm{De}\,\tau_{rr} + \alpha)\frac{D}{Dt}(\ln(F)) - \alpha\frac{\partial w}{\partial z}. \tag{32}$$

It is now convenient to transform to Lagrangian coordinates, so we let

$$\zeta = \int_0^{Z(\zeta,t)} R^2(z,t)\,\mathrm{d}z, \qquad R(Z(\zeta,t),t) = \tilde{R}(\zeta,t), \qquad etc. \tag{33}$$

When we drop the ˜s we obtain

$$\frac{\partial w}{\partial \zeta} = \frac{\partial}{\partial t}\left(\frac{1}{R^2}\right), \tag{34}$$

$$T(t) = R^2\left(\tau_{zz} - \tau_{rr} + 3\beta R^2\frac{\partial w}{\partial \zeta}\right)\Big), \tag{35}$$

$$F\tau_{zz} + \mathrm{De}\left(\frac{\partial \tau_{zz}}{\partial t} - 2R^2\tau_{zz}\frac{\partial w}{\partial \zeta}\right) = (\mathrm{De}\,\tau_{zz} + \alpha)\frac{\partial}{\partial t}(\ln(F)) + 2\alpha R^2\frac{\partial w}{\partial \zeta}, \tag{36}$$

$$F\tau_{rr} + \mathrm{De}\left(\frac{\partial \tau_{rr}}{\partial t} + R^2\tau_{rr}\frac{\partial w}{\partial \zeta}\right) = (\mathrm{De}\,\tau_{rr} + \alpha)\frac{\partial}{\partial t}(\ln(F)) - \alpha R^2\frac{\partial w}{\partial \zeta}, \tag{37}$$

with

$$l(t) = w(1,t) = \int_0^1 \frac{\mathrm{d}\zeta}{R(\zeta,t)^2}. \tag{38}$$

Note that $\partial Z/\partial t = w$.

Assuming now a uniform filament thickness $R = R(t)$, $l(t) = 1/R(t)^2$, we have

$$T(t) = R^2\left(\tau_{zz} - \tau_{rr} + 3\beta R^2\frac{\mathrm{d}}{\mathrm{d}t}\left(\frac{1}{R^2}\right)\right), \tag{39}$$

$$F\tau_{zz} + \mathrm{De}\left(\frac{\mathrm{d}\tau_{zz}}{\mathrm{d}t} - 2R^2\tau_{zz}\frac{\mathrm{d}}{\mathrm{d}t}\left(\frac{1}{R^2}\right)\right) = (\mathrm{De}\,\tau_{zz} + \alpha)\frac{\mathrm{d}}{\mathrm{d}t}(\ln(F)) + 2\alpha R^2\frac{\mathrm{d}}{\mathrm{d}t}\left(\frac{1}{R^2}\right), \tag{40}$$

$$F\tau_{rr} + \mathrm{De}\left(\frac{\mathrm{d}\tau_{rr}}{\mathrm{d}t} + R^2\tau_{rr}\frac{\mathrm{d}}{\mathrm{d}t}\left(\frac{1}{R^2}\right)\right) = (\mathrm{De}\,\tau_{rr} + \alpha)\frac{\mathrm{d}}{\mathrm{d}t}(\ln(F)) - \alpha\frac{\mathrm{d}}{\mathrm{d}t}\left(\frac{1}{R^2}\right), \tag{41}$$

where

$$F = 1 + \frac{3}{b}\left(1 + \frac{\mathrm{De}}{3}(2\tau_{rr} + \tau_{zz})\right). \tag{42}$$

Some numerical results from this model have been obtained by taking

$$b = 50, \quad \beta = \frac{0.0015}{0.68}, \quad \mathrm{De} = 80. \tag{43}$$

The total tension during an extension, and the contributions of polymer and solvent to that total are shown in Figure 9. The behaviour of τ_{rr} and τ_{zz} during the extension are shown in Figure 10.

In summary, this analysis of a FENE-P extensional filament is intended to model the later stages of the experiment when the sphere is connected to the substrate by a slender viscoelastic filament. However, we find that the force is only of correct order of magnitude if the thread volume is more than is suggested by the simple volume calculation (3). This suggests that the process by which the squeeze film sucks additional fluid into the contact region is important. Further important open questions include stability and pinch off. The early stages of the pull-off are perhaps better dealt with using the theory of the Maxwell viscoelastic inverse squeeze film.

6 Lumped parameter model

When we put together the lubrication force F_l from (6) and the filament force $F_f = T$ from (39) and impose a steadily increasing applied separation Vt we have

$$k\Delta = k(Vt + h_0(0) - h_0) = F = F_l + F_f. \tag{44}$$

Letting

$$\hat{h}_0 = h_0/h_0(0), \quad \hat{t} = Vt/h_0(0), \tag{45}$$

and then immediately dropping the $\hat{}$, we may write

$$c(t + 1 - h_0) = \frac{\dot{h}_0}{h_0}\frac{d^4}{h_0^4 + \frac{1}{4}d^4} + \frac{2\epsilon^2}{3\pi\beta}\frac{1}{h_0}\left(\tau_{zz} + \frac{3\beta}{h_0}\dot{h}_0\right), \tag{46}$$

where

$$c \equiv \frac{2k\epsilon^2}{3\pi\mu_s V}, \quad \epsilon \equiv \frac{h_0(0)}{R} \tag{47}$$

and all other parameters are as defined in Section 5. In the one-dimensional approximation used here, the viscoelastic model of Section 5 (equation (40)) shows that τ_{zz} evolves according to

$$F\tau_{zz} + \mathrm{De}\left(\dot{\tau}_{zz} - \frac{2}{h_0}\dot{h}_0\tau_{zz}\right) = \left(\mathrm{De}\tau_{zz} + \frac{b}{b+2}\right)\frac{\dot{F}}{F} + \frac{2b}{b+2}\frac{\dot{h}_0}{h_0}, \tag{48}$$

where F is given in (42). The coupled ordinary differential equations (46) and (48) can easily be solved numerically to give h_0 and τ_{zz} as functions of time. These yield force-separation curves, an example of which is shown in Figure 11 using the representative data given in Appendix B and $c = 0.5$, $d = 20$ and $\epsilon = 0.047$. There was considerable uncertainty and confusion during the Study Group as to what the real values of these last three parameters were for the available experimental data. If Unilever could have provided a checked data table, that would have been a great help.

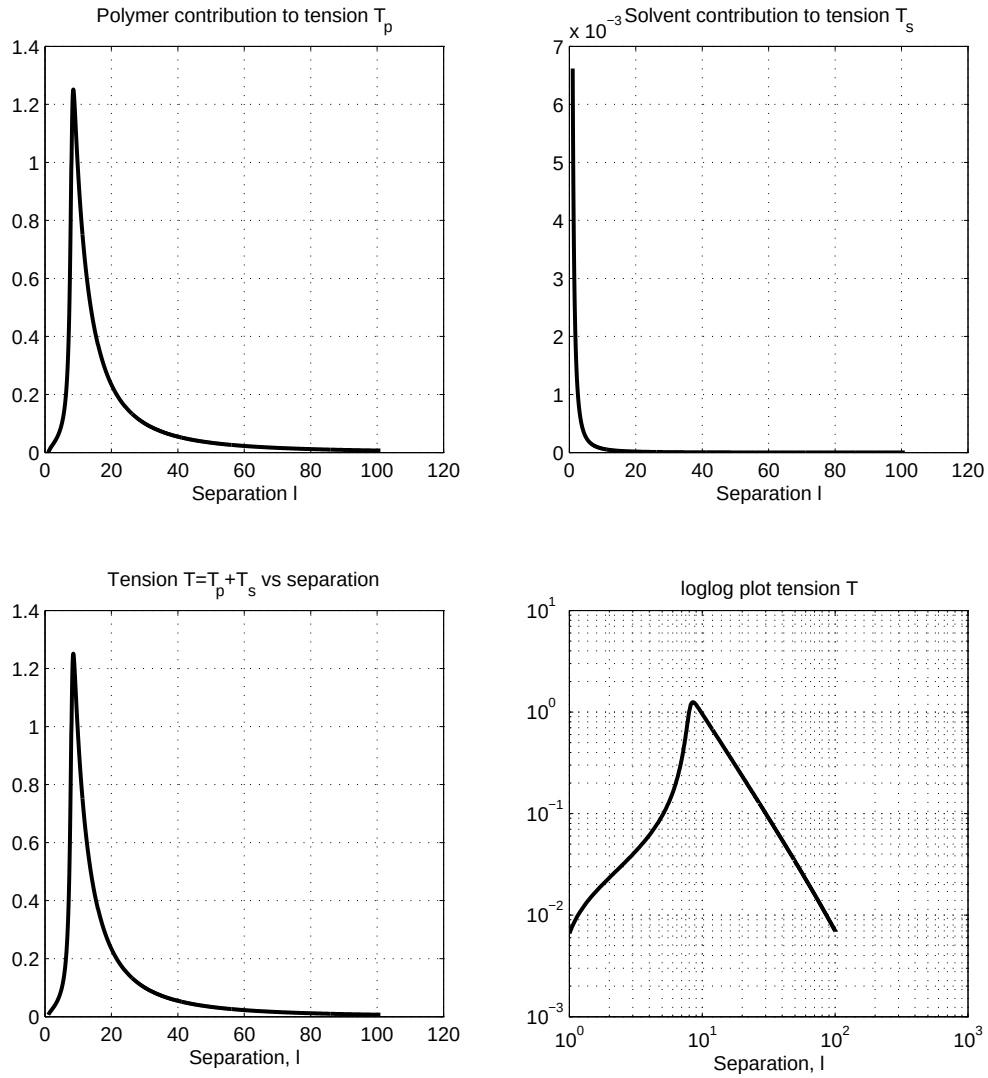

Figure 9: Nonlinear viscoelastic extension of a FENE-P filament. Contributions of polymer and solvent to the tension (top left and right). Total tension plotted against separation on linear (bottom left) and logarithmic (bottom right) scales.

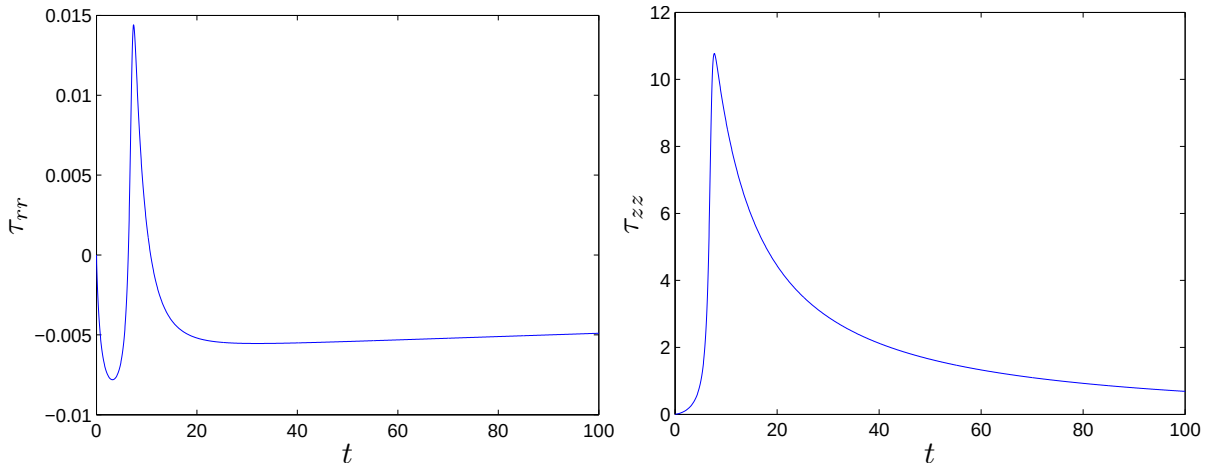

Figure 10: Behaviour of τ_{rr} and τ_{zz} during the extension shown in Figure 9.

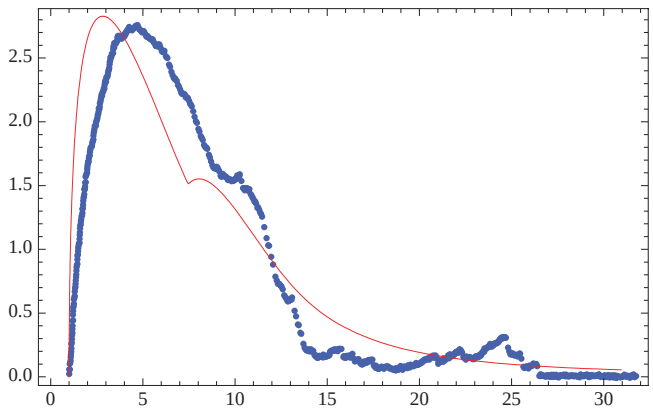

Figure 11: Dimensionless response of experiment (blue dots) and model (red curve).

7 Conclusions and further work

The modelling here has put together a linear model for the squeeze film and a fully nonlinear (FENE-P) model for the filament to produce a lumped parameter model for the AFM that has response curves agreeing with measurements. The more difficult nonlinear model of the squeeze film has been opened up by the analysis in Appendix A and is ready to be taken further.

The elastic and adhesive forces were not studied in much detail, but there is some information available that could be used to work on these.

The standard (Hertz) theory of elastic contact implies that the elastic deflections of a glass sphere and substrate would be small compared to the other deflections involved. However, for a softer substrate that will obviously change considerably and should be analysed again.

The electrostatic data supplied is listed in Appendix B. For the adhesive case, the resulting electrostatic force between a rigid sphere coated with chitosan and plane substrate coated with polyelectrolyte can then be calculated. It does not appear to be as great as the apparent adhesive force observed in some of the experiments. This is presumably due to the fact that the elasticity of the materials enables close contact to be achieved over a larger effective area than for rigid bodies.

A Nonlinear squeeze film analysis

As mentioned earlier the analysis of a fully nonlinear squeeze film has been begun but not carried through to its final conclusions. We present in this section what has been done. The main message is that the stress field is dominated by a slowly relaxing elastic model, in which the strains may be approximated using the thinness of the layer. It is not clear how to take the analysis here much further analytically, but numerical studies with realistic parameter values could be illuminating.

A.1 Introduction

In each of the squeezing, retraction and final filament extension phases of the process, motions may be treated as axisymmetric (although stability may be an issue during retraction and inward radial flow). Unilever are trying to determine parameters within a FENE-P model with parameter λ (a relaxation time) ≈ 250 secs. Moreover, it appears that during much of the deformation process, (visco-)elastic stresses predominate over viscous stresses in determining the deformation and flow field. Even with dimensions suggesting a squeeze-film analysis, familiar parabolic distributions of velocity are inappropriate. The following treatment is offered as a step towards developing a thin film analysis.

A.2 The FENE-P model

The constitutive equation for the Cauchy stress $\bar{\boldsymbol{\sigma}}$ is taken as

$$\bar{\boldsymbol{\sigma}} = \boldsymbol{\tau}_{\rm tot} \equiv -\bar{p}\boldsymbol{\delta} + \eta_s[\boldsymbol{\nabla}\mathbf{u} + (\boldsymbol{\nabla}\mathbf{u})^T] + \bar{\boldsymbol{\tau}}\,, \tag{49}$$

where $\mathbf{u}$ is the velocity, $\boldsymbol{\delta}$ is the unit tensor, ^{T} denotes a transpose, p is a hydrostatic pressure and η_s a viscosity (bars distinguish physical dimensional quantities from non-dimensional quantities used later). The contribution $\bar{\boldsymbol{\tau}}$ to the stress evolves with time according to

$$F\bar{\boldsymbol{\tau}} + \lambda\left[\bar{\boldsymbol{\tau}}_{(1)} - \frac{1}{F}\frac{{\rm D}F}{{\rm D}\bar{t}}\bar{\boldsymbol{\tau}}\right] = \frac{b}{b+2}\eta_p\left[\boldsymbol{\nabla}\mathbf{u} + (\boldsymbol{\nabla}\mathbf{u})^T + \frac{1}{F}\frac{{\rm D}F}{{\rm D}\bar{t}}\boldsymbol{\delta}\right]\,, \tag{50}$$

where $b = 50$, ${\rm D}/{\rm D}\bar{t}$ denotes the material (or advective) derivative $\partial/\partial\bar{t} + \mathbf{u}\cdot\boldsymbol{\nabla}$ and $_{(1)}$ denotes the Jaumann derivative defined by

$$\bar{\boldsymbol{\tau}}_{(1)} \equiv \frac{{\rm D}\bar{\boldsymbol{\tau}}}{{\rm D}\bar{t}} - \left[(\boldsymbol{\nabla}\mathbf{u})\cdot\bar{\boldsymbol{\tau}} + \bar{\boldsymbol{\tau}}\cdot(\boldsymbol{\nabla}\mathbf{u})^T\right]\,. \tag{51}$$

Both $\bar{\boldsymbol{\sigma}}$ and $\bar{\boldsymbol{\tau}}$ are symmetric and the scalar F is given by

$$F \equiv 1 + b^{-1}[3 + (\lambda/\eta_p)\,{\rm Tr}\,\bar{\boldsymbol{\tau}}]\,. \tag{52}$$

We observe that since $\boldsymbol{\delta}_{(1)} = -[\boldsymbol{\nabla}\mathbf{u} + (\boldsymbol{\nabla}\mathbf{u})^T]$, a balance between the bracketed terms on the left- and right-hand sides of (50) (perhaps relevant on time scales short compared to λ) is provided by $\bar{\boldsymbol{\tau}} = -(\alpha\eta_p/\lambda)\boldsymbol{\delta}$, where $\alpha \equiv b/(b+2) \approx 0.96$.

However, equation (50) may be analysed in greater generality by using Lagrangian coordinates as follows in section A.3.

A.3 Time-evolution of $\bar{\boldsymbol{\tau}}$

Let $\bar{x}_i$ $(i = 1, 2, 3)$ denote Eulerian coordinates and $\bar{X}_J$ $(J = 1, 2, 3)$ denote Lagrangian coordinates, so that a deformation $\bar{\mathbf{X}} \to \bar{\mathbf{x}}(\bar{\mathbf{X}}, \bar{t})$ has velocity $\mathbf{u}$ and deformation-gradient tensor $\mathbf{F}$ with components $u_i \equiv \partial\bar{x}_i/\partial\bar{t}$ and $F_{iJ} \equiv \partial\bar{x}_i/\partial\bar{X}_J$, respectively. Then,

$$\dot{F}_{iJ} \equiv \frac{\partial}{\partial\bar{t}}\left(\frac{\partial\bar{x}_i}{\partial\bar{X}_J}\right) = \frac{\partial u_i}{\partial\bar{X}_J} = \frac{\partial u_i}{\partial\bar{x}_k}\frac{\partial\bar{x}_k}{\partial\bar{X}_J}\,, \tag{53}$$

or

$$\dot{\mathbf{F}} = (\boldsymbol{\nabla}\mathbf{u})\cdot\mathbf{F}\,, \qquad \text{so that} \quad \dot{\mathbf{F}}^T = \mathbf{F}^T\cdot(\boldsymbol{\nabla}\mathbf{u})^T\,, \quad \text{where } \dot{} \equiv \frac{\rm D}{{\rm D}\bar{t}}\,. \tag{54}$$

Now, write $\bar{\boldsymbol{\tau}} \equiv \mathbf{F}\cdot\bar{\mathbf{T}}\cdot\mathbf{F}^T$, so that $\bar{\mathbf{T}} = \mathbf{F}^{-1}\cdot\bar{\boldsymbol{\tau}}\cdot(\mathbf{F}^T)^{-1}$ is the second Piola stress and is symmetric. This gives

$$\frac{{\rm D}\bar{\boldsymbol{\tau}}}{{\rm D}\bar{t}} = \dot{\mathbf{F}}\cdot\mathbf{F}^{-1}\cdot\bar{\boldsymbol{\tau}} + \mathbf{F}\cdot\frac{{\rm D}\bar{\mathbf{T}}}{{\rm D}\bar{t}}\cdot\mathbf{F}^T + \bar{\boldsymbol{\tau}}\cdot(\mathbf{F}^T)^{-1}\cdot\dot{\mathbf{F}}^T = (\boldsymbol{\nabla}\mathbf{u})\cdot\bar{\boldsymbol{\tau}} + \bar{\boldsymbol{\tau}}\cdot(\boldsymbol{\nabla}\mathbf{u})^T + \mathbf{F}\cdot\frac{{\rm D}\bar{\mathbf{T}}}{{\rm D}\bar{t}}\cdot\mathbf{F}^T \tag{55}$$

so that

$$\frac{\mathrm{D}\bar{\mathbf{T}}}{\mathrm{D}\bar{t}} = \mathbf{F}^{-1}\cdot\bar{\boldsymbol{\tau}}_{(1)}\cdot(\mathbf{F}^{T})^{-1}\,. \tag{56}$$

Using the observation at the end of section A.2, it is readily confirmed that

$$\frac{\mathrm{D}}{\mathrm{D}\bar{t}}[\mathbf{F}^{-1}\cdot(\mathbf{F}^{T})^{-1}] = -\mathbf{F}^{-1}\cdot\dot{\mathbf{F}}(\mathbf{F}^{T}\mathbf{F})^{-1} - (\mathbf{F}^{T}\mathbf{F})^{-1}\cdot\dot{\mathbf{F}}^{T}\cdot(\mathbf{F}^{T})^{-1} \tag{57}$$

$$= -\mathbf{F}^{-1}\cdot[\boldsymbol{\nabla}\mathbf{u} + (\boldsymbol{\nabla}\mathbf{u})^{T}]\cdot(\mathbf{F}^{T})^{-1}\,. \tag{58}$$

Hence, equation (50) may be rearranged as

$$\lambda\left(\frac{\mathrm{D}\bar{\mathbf{T}}}{\mathrm{D}\bar{t}} - \frac{1}{F}\frac{\mathrm{D}F}{\mathrm{D}\bar{t}}\bar{\mathbf{T}}\right) + F\bar{\mathbf{T}} = -\alpha\eta_{p}\left(\frac{\mathrm{D}}{\mathrm{D}\bar{t}}[\mathbf{G}^{-1}] - \frac{1}{F}\frac{\mathrm{D}F}{\mathrm{D}\bar{t}}\mathbf{G}^{-1}\right)\,, \tag{59}$$

where $\mathbf{G}\equiv\mathbf{F}^{T}\cdot\mathbf{F}$ is the Cauchy-Green strain, or as

$$\lambda\frac{\mathrm{D}}{\mathrm{D}\bar{t}}(\bar{\mathbf{T}}/F) + \alpha\eta_{p}\frac{\mathrm{D}}{\mathrm{D}\bar{t}}[\mathbf{G}^{-1}/F] + \bar{\mathbf{T}} = \mathbf{0}\,. \tag{60}$$

Equation (60) is then an evolution equation for the symmetric stress $\bar{\mathbf{T}}$ at each material point $\bar{\mathbf{X}}=$ constant, in terms of the history of the (symmetric) Cauchy-Green strain and of the scalar F. Although F evolves along with $\bar{\mathbf{T}}$ (since equation (52) gives F in terms of $\mathrm{Tr}\,\mathbf{F}\cdot\bar{\mathbf{T}}\cdot\mathbf{F}^{T}$), if the size of b makes $F\approx 1$ then equation (60) is much simplified as

$$\frac{\mathrm{D}\bar{\mathbf{T}}}{\mathrm{D}\bar{t}} + \gamma\frac{\mathrm{D}}{\mathrm{D}\bar{t}}\mathbf{G}^{-1} + \lambda^{-1}\bar{\mathbf{T}} = \mathbf{0}\,, \tag{61}$$

for which the solution may be written as

$$\bar{\mathbf{T}}(\bar{\mathbf{X}},\bar{t}) = \gamma[\boldsymbol{\delta} - \mathbf{G}^{-1}(\bar{\mathbf{X}},\bar{t})]\mathrm{e}^{-\bar{t}/\lambda} + \frac{\gamma}{\lambda}\int_{0}^{\bar{t}}[\mathbf{G}^{-1}(\bar{\mathbf{X}},s) - \mathbf{G}^{-1}(\bar{\mathbf{X}},\bar{t})]\mathrm{e}^{(s-\bar{t})/\lambda}\mathrm{d}s\,, \tag{62}$$

where $\gamma\equiv\alpha\eta_{p}/\lambda$. However, the $_{JM}$ component of $\mathbf{G}^{-1}$ is $\boldsymbol{\nabla}\bar{X}_{J}\cdot\boldsymbol{\nabla}\bar{X}_{M}$, so that, after defining $\mathbf{g}\equiv\mathbf{F}\cdot\mathbf{F}^{T}$, this solution (62) may be rearranged for $\bar{\boldsymbol{\tau}}$ in the form

$$(\bar{\boldsymbol{\tau}})_{ij} = \gamma\mathrm{e}^{-\bar{t}/\lambda}\left\{g_{ij}(\bar{\mathbf{X}},\bar{t}) - \delta_{ij} + \lambda^{-1}\int_{0}^{\bar{t}}\mathrm{e}^{s/\lambda}\left[\frac{\partial\bar{x}_{i}(t)}{\partial\bar{x}_{k}(s)}\frac{\partial\bar{x}_{j}(t)}{\partial\bar{x}_{k}(s)} - \delta_{ij}\right]\mathrm{d}s\right\}\,, \tag{63}$$

with all positions $\bar{\mathbf{x}}$ evaluated at a fixed particle $\bar{\mathbf{X}}=$ constant. This emphasises that the current values of the stress components depend upon the history of strain relative to *all* earlier configurations (it has been assumed that the material was static and unstressed for $\bar{t}<0$). Only when the configuration changes on a time scale long compared to λ can $\bar{\boldsymbol{\tau}}$ be approximated as a function of the current strain rate. Indeed, for changes of configuration taking place over times $\ll\lambda$, then $\bar{\mathbf{T}}\approx\gamma(\boldsymbol{\delta}-\mathbf{G}^{-1})\mathrm{e}^{-\bar{t}/\lambda}$ so that the stress $\bar{\boldsymbol{\tau}}$ is approximated by $\gamma(\mathbf{g}-\boldsymbol{\delta})\mathrm{e}^{-\bar{t}/\lambda}$, which may itself be approximated for times $\ll\lambda$ by the nonlinear elastic response $\bar{\boldsymbol{\tau}}=\gamma(\mathbf{g}-\boldsymbol{\delta})$. Accordingly, a squeeze film analysis must involve analysis of *displacement gradients* as well as of strain rates.

A.4 Axially-symmetric thin layer deformation

In terms of (physical) cylindrical polar coordinates $(\bar{r}, \theta, \bar{z})$, their Lagrangian equivalents $(\bar{R}, \theta, \bar{Z})$ and time $\bar{t}$, the deformation gradient $\mathbf{F}$ and Cauchy stress $\bar{\boldsymbol{\sigma}}$ for axial symmetry are (commas denoting partial differentiation)

$$\mathbf{F} = \mathbf{H} \cdot \begin{pmatrix} \bar{r}_{,\bar{R}} & 0 & \bar{r}_{,\bar{Z}} \\ 0 & \bar{r}/\bar{R} & 0 \\ \bar{z}_{,\bar{R}} & 0 & \bar{z}_{,\bar{Z}} \end{pmatrix} \cdot \mathbf{H}^T \equiv \mathbf{H} \cdot \mathbf{P} \cdot \mathbf{H}^T ; \tag{64}$$

$$\bar{\boldsymbol{\sigma}} = \mathbf{H} \cdot \begin{pmatrix} \bar{\sigma}_{rr} & 0 & \bar{\sigma}_{rz} \\ 0 & \bar{\sigma}_{\theta\theta} & 0 \\ \bar{\sigma}_{zr} & 0 & \bar{\sigma}_{zz} \end{pmatrix} \cdot \mathbf{H}^T \equiv \mathbf{H} \cdot \hat{\boldsymbol{\sigma}} \cdot \mathbf{H}^T , \tag{65}$$

where $\bar{\sigma}_{zr} = \bar{\sigma}_{rz}$ $(i.e.\ \hat{\boldsymbol{\sigma}}^T = \hat{\boldsymbol{\sigma}})$ and

$$\mathbf{H} \equiv \begin{pmatrix} \cos\theta & -\sin\theta & 0 \\ \sin\theta & \cos\theta & 0 \\ 0 & 0 & 1 \end{pmatrix} \quad \text{with} \quad \mathbf{H} \cdot \mathbf{H}^T = \boldsymbol{\delta} . \tag{66}$$

Then $\boldsymbol{\nabla}\mathbf{u} = \mathbf{H} \cdot \dot{\mathbf{P}} \cdot \mathbf{P}^{-1} \cdot \mathbf{H}^T$,

$$\mathbf{P}^{-1} = \frac{\bar{r}}{\bar{R}} \begin{pmatrix} \bar{z}_{,\bar{Z}} & 0 & -\bar{r}_{,\bar{Z}} \\ 0 & (\bar{R}/\bar{r})^2 & 0 \\ -\bar{z}_{,\bar{R}} & 0 & \bar{r}_{,\bar{R}} \end{pmatrix} \tag{67}$$

and $(\bar{r}_{,\bar{R}}\bar{z}_{,\bar{Z}} - \bar{r}_{,\bar{Z}}\bar{z}_{,\bar{R}})\bar{r}/\bar{R} = \det \mathbf{P} = +1$.

In the Eulerian formulation, $\bar{R}$ and $\bar{Z}$ are treated as functions of $\bar{r}$, $\bar{z}$ and $\bar{t}$ and the components $\bar{u}$ and $\bar{w}$ of velocity $\mathbf{u} = \bar{u}\mathbf{e}_r + \bar{w}\mathbf{e}_z$ are given by

$$\bar{u} = (\bar{R}/\bar{r})(\bar{R}_{,\bar{z}}\bar{Z}_{,\bar{t}} - \bar{Z}_{,\bar{z}}\bar{R}_{,\bar{t}}) , \qquad \bar{w} = (\bar{R}/\bar{r})(\bar{R}_{,\bar{t}}\bar{Z}_{,\bar{r}} - \bar{Z}_{,\bar{t}}\bar{R}_{,\bar{r}}) , \tag{68}$$

while, since $\bar{r}_{,\bar{R}} = (\bar{R}/\bar{r})\bar{Z}_{,\bar{z}}$, $\bar{r}_{,\bar{Z}} = -(\bar{R}/\bar{r})\bar{R}_{,\bar{z}}$, $\bar{z}_{,\bar{R}} = -(\bar{R}/\bar{r})\bar{Z}_{,\bar{r}}$ and $\bar{z}_{,\bar{Z}} = (\bar{R}/\bar{r})\bar{R}_{,\bar{r}}$, the matrices $\mathbf{P}$ and $\mathbf{P}^{-1}$ become

$$\mathbf{P} = \frac{\bar{R}}{\bar{r}} \begin{pmatrix} \bar{Z}_{,\bar{z}} & 0 & -\bar{R}_{,\bar{z}} \\ 0 & (\bar{r}/\bar{R})^2 & 0 \\ -\bar{Z}_{,\bar{r}} & 0 & \bar{R}_{,\bar{r}} \end{pmatrix} \quad \text{and} \quad \mathbf{P}^{-1} = \begin{pmatrix} \bar{R}_{,\bar{r}} & 0 & \bar{R}_{,\bar{z}} \\ 0 & \bar{R}/\bar{r} & 0 \\ \bar{Z}_{,\bar{r}} & 0 & \bar{Z}_{,\bar{z}} \end{pmatrix} . \tag{69}$$

Writing the (physical) cylindrical polar components of Cauchy stress $\hat{\boldsymbol{\sigma}}$ as

$$\hat{\boldsymbol{\sigma}} \equiv \begin{pmatrix} \bar{\sigma}_{rr} & 0 & \bar{\sigma}_{rz} \\ 0 & \bar{\sigma}_{\theta\theta} & 0 \\ \bar{\sigma}_{zr} & 0 & \bar{\sigma}_{zz} \end{pmatrix} = \mathbf{H}^T \cdot \bar{\boldsymbol{\sigma}} \cdot \mathbf{H} = -\bar{p}\boldsymbol{\delta} + \eta_s[\dot{\mathbf{P}} \cdot \mathbf{P}^{-1} + (\dot{\mathbf{P}} \cdot \mathbf{P}^{-1})^T] + \hat{\boldsymbol{\tau}} \tag{70}$$

where $\bar{\boldsymbol{\tau}}^T = \bar{\boldsymbol{\tau}}$ with

$$\hat{\boldsymbol{\tau}} \equiv \begin{pmatrix} \bar{\tau}_{rr} & 0 & \bar{\tau}_{rz} \\ 0 & \bar{\tau}_{\theta\theta} & 0 \\ \bar{\tau}_{zr} & 0 & \bar{\tau}_{zz} \end{pmatrix} = \mathbf{H}^T \cdot \bar{\boldsymbol{\tau}} \cdot \mathbf{H} \ \text{ so that } \qquad \bar{\boldsymbol{\tau}} = \mathbf{H} \cdot \hat{\boldsymbol{\tau}} \cdot \mathbf{H}^T \tag{71}$$

satisfies

$$\mathbf{H}^T \cdot \bar{\boldsymbol{\tau}}_{(1)} \cdot \mathbf{H} = \frac{\mathrm{D}\hat{\boldsymbol{\tau}}}{\mathrm{D}\bar{t}} - [\dot{\mathbf{P}} \cdot \mathbf{P}^{-1} \cdot \hat{\boldsymbol{\tau}} + \hat{\boldsymbol{\tau}} \cdot (\mathbf{P}^T)^{-1} \cdot (\dot{\mathbf{P}})^T] \,. \tag{72}$$

Just as equation (50) may be interpreted more simply as an equation for $\bar{\mathbf{T}} \equiv \mathbf{F}^{-1} \cdot \bar{\boldsymbol{\tau}} \cdot (\mathbf{F}^T)^{-1}$, the evolution of cylindrical polar components is best written in terms of $\hat{\mathbf{T}} \equiv \mathbf{P}^{-1} \cdot \hat{\boldsymbol{\tau}} \cdot (\mathbf{P}^T)^{-1} = \hat{\mathbf{T}}^T$ (such that $\hat{\boldsymbol{\tau}} = \mathbf{P} \cdot \hat{\mathbf{T}} \cdot \mathbf{P}^T$) as

$$\frac{\mathrm{D}}{\mathrm{D}\bar{t}} \left(\frac{\hat{\mathbf{T}}}{F} + \gamma (\mathbf{P}^T \cdot \mathbf{P})^{-1} \right) + \lambda^{-1} \hat{\mathbf{T}} = \mathbf{0} \,, \tag{73}$$

with $\gamma \equiv \alpha \eta_p / \lambda$ as before and with $F = 1 + 3b^{-1} + \gamma^{-1}(\bar{\tau}_{rr} + \bar{\tau}_{\theta\theta} + \bar{\tau}_{zz})/(b+2)$.

A.5 Scalings

For a sphere of radius a squeezing a mucous film of initial radius h ($\ll a$), define $h/a = \varepsilon^2$ so that the contact zone has radius comparable with $\sqrt{ha} = \varepsilon a = \varepsilon^{-1} h \equiv L$. Dimensionless variables are introduced by writing

$$\bar{r} = Lr \,,\ \bar{z} = hz = \varepsilon L z \,;\ \bar{R} = LR \,,\ \bar{Z} = hZ = \varepsilon L Z \,;\ \bar{t} = LU^{-1} t \tag{74}$$

where U is a typical speed, so that $\bar{u} = Uu$, $\bar{w} = \varepsilon U w$. This rescaling gives

$$\mathbf{P} = \begin{pmatrix} cZ_{,z} & 0 & -\varepsilon^{-1} c R_{,z} \\ 0 & c^{-1} & 0 \\ -\varepsilon c Z_{,r} & 0 & c R_{,r} \end{pmatrix} ; \quad \mathbf{P}^{-1} = \begin{pmatrix} R_{,r} & 0 & \varepsilon^{-1} R_{,z} \\ 0 & c & 0 \\ \varepsilon Z_{,r} & 0 & Z_{,z} \end{pmatrix} , \tag{75}$$

$$u = c(R_{,z} Z_{,t} - R_{,t} Z_{,z}) \ , \qquad w = c(Z_{,r} R_{,t} - R_{,r} Z_{,t}) \,, \tag{76}$$

where $c \equiv R/r = c(r,z,t)$. These expressions for u and w automatically satisfy the continuity equation $r^{-1}(ru)_{,r} + w_{,z} = 0$ since incompressibility gives $R\partial(R,Z)/\partial(r,z) = r$.

A.6 Euler equations

Neglect of inertial and body forces yields the equilibrium equations

$$\frac{\partial \bar{\sigma}_{rr}}{\partial r} + \frac{\bar{\sigma}_{rr} - \bar{\sigma}_{\theta\theta}}{r} + \varepsilon^{-1} \frac{\partial \bar{\sigma}_{rz}}{\partial z} = 0 \tag{77}$$

$$\frac{1}{r} \frac{\partial}{\partial r} (r \bar{\sigma}_{rz}) + \varepsilon^{-1} \frac{\partial \bar{\sigma}_{zz}}{\partial z} = 0 \,. \tag{78}$$

Since

$$\dot{\mathbf{P}} \cdot \mathbf{P}^{-1} = \mathbf{H}^T \cdot \boldsymbol{\nabla} \mathbf{u} \cdot \mathbf{H} = \begin{pmatrix} \bar{u}_{,\bar{r}} & 0 & \bar{u}_{,\bar{z}} \\ 0 & \bar{u}/\bar{r} & 0 \\ \bar{w}_{,\bar{r}} & 0 & \bar{w}_{,\bar{z}} \end{pmatrix} = \frac{U}{L} \begin{pmatrix} u_{,r} & 0 & \varepsilon^{-1} u_{,z} \\ 0 & u/r & 0 \\ \varepsilon w_{,r} & 0 & w_{,z} \end{pmatrix} , \tag{79}$$

the stress components given by (70) are

$$\bar{\sigma}_{rr} = -\bar{p} + 2\frac{\eta_s U}{L}u_{,r} + \bar{\tau}_{rr} \quad , \qquad \bar{\sigma}_{rz} = \bar{\sigma}_{zr} = \frac{\eta_s U}{L}(\varepsilon^{-1}u_{,z} + \varepsilon w_{,r}) + \bar{\tau}_{rz}\,, \tag{80}$$

$$\bar{\sigma}_{\theta\theta} = -\bar{p} + 2\frac{\eta_s U}{L}\frac{u}{r} + \bar{\tau}_{\theta\theta} \quad , \qquad \bar{\sigma}_{zz} = -\bar{p} + 2\frac{\eta_s U}{L}w_{,z} + \bar{\tau}_{zz}\,. \tag{81}$$

Then, using the definitions $\eta_s/\eta_p \equiv \beta \approx 2\times 10^{-3}$ (*i.e.* small), $\mathrm{De} = \lambda U/L$, $\bar{p} = \eta_p p/\lambda$, $(\bar{\tau}_{rr}, \bar{\tau}_{rz}, \bar{\tau}_{\theta\theta}, \bar{\tau}_{zz}) = (\eta_p/\lambda)(\tau_{rr}, \tau_{rz}, \tau_{\theta\theta}, \tau_{zz})$ and $\hat{\mathbf{T}} = (\eta_p/\lambda)\mathbf{T}$ yields the equilibrium equations

$$\frac{\partial}{\partial z}[\tau_{rz} + \nu(\varepsilon^{-1}u_{,z} + \varepsilon w_{,r})] + \varepsilon\frac{\partial}{\partial r}(\tau_{rr} - p) + \varepsilon\frac{\tau_{rr} - \tau_{\theta\theta}}{r} + 2\varepsilon\nu\frac{\partial}{\partial r}\left(\frac{1}{r}\frac{\partial(ru)}{\partial r}\right) = 0\,, \tag{82}$$

$$\frac{\partial}{\partial z}(\tau_{zz} - p + 2\nu w_{,z}) + \frac{\nu}{r}\frac{\partial}{\partial r}(ru_{,z} + \varepsilon^2 r w_{,r}) + \frac{\varepsilon}{r}\frac{\partial}{\partial r}(r\tau_{rz}) = 0\,, \tag{83}$$

where $\nu \equiv \beta\mathrm{De}$. Also, the stress evolution equation (73) becomes

$$\frac{\mathrm{D}}{\mathrm{D}t}\left(\frac{\mathbf{T}}{F} + \alpha(\mathbf{P}^T\cdot\mathbf{P})^{-1}\right) + \frac{1}{\mathrm{De}}\mathbf{T} = \mathbf{0}\,. \tag{84}$$

Motivated by the approximation $\hat{\boldsymbol{\tau}} \approx \gamma \mathrm{e}^{-t/\mathrm{De}}(\mathbf{P}\cdot\mathbf{P}^T - \boldsymbol{\delta})$ (following from (63)) so that

$$\tau_{rr} \approx \alpha\mathrm{e}^{-t/\mathrm{De}}\{c^2[(Z_{,z})^2 + \varepsilon^{-2}(R_{,z})^2] - 1\}\,,\ \tau_{rz} \approx -\alpha\mathrm{e}^{-t/\mathrm{De}}c^2(\varepsilon^{-1}R_{,r}R_{,z} + \varepsilon Z_{,r}Z_{,z})\,, \tag{85}$$

$$\tau_{\theta\theta} \approx \alpha\mathrm{e}^{-t/\mathrm{De}}(c^{-2} - 1)\,, \qquad \tau_{zz} \approx \alpha\mathrm{e}^{-t/\mathrm{De}}\{c^2[(R_{,r})^2 + \varepsilon^2(Z_{,r})^2] - 1\} \tag{86}$$

and the fact that $R_{,r} = \mathrm{O}(1)$, these motivate the fact that $\tau_{rr} = \mathrm{O}(\varepsilon^{-2})$ and $\tau_{rz} = \mathrm{O}(\varepsilon^{-1})$ — the shear strain makes large contributions not only to the shear stress, but also to the radial stress. This can be seen as a consequence of material rotation, whereby short material elements initially normal to the layer are substantially lengthened as they become aligned almost parallel to the layer.

Thus, writing $\tau_{rr} = \varepsilon^{-2}s_{rr}$, $\tau_{rz} = \varepsilon^{-1}s_{rz}$, $T_{rr} = \varepsilon^{-2}S_{rr}$ and $T_{rz} = \varepsilon^{-1}S_{rz}$ yields the leading order equilibrium equations

$$\frac{\partial s_{rr}}{\partial r} + \frac{\partial}{\partial z}\left(s_{rz} + \nu\frac{\partial u}{\partial z}\right) = \mathrm{O}(\varepsilon)\,, \quad \frac{\partial}{\partial z}(\tau_{zz} - p) + \frac{1}{r}\frac{\partial}{\partial r}(rs_{rz}) = \mathrm{O}(\nu,\varepsilon)\,. \tag{87}$$

The scaled components of second Piola stress evolve according to

$$\frac{\mathrm{D}}{\mathrm{D}t}\left(\frac{S_{rr}}{F} + \alpha[(R_{,z})^2 + \varepsilon^2(R_{,r})^2]\right) + \frac{1}{\mathrm{De}}S_{rr} = 0\,, \tag{88}$$

$$\frac{\mathrm{D}}{\mathrm{D}t}\left(\frac{S_{rz}}{F} + \alpha(Z_{,z}R_{,z} + \varepsilon^2 R_{,r}Z_{,z})\right) + \frac{1}{\mathrm{De}}S_{rz} = 0\,, \tag{89}$$

$$\frac{\mathrm{D}}{\mathrm{D}t}\left(\frac{T_{\theta\theta}}{F} + \alpha c^2\right) + \frac{1}{\mathrm{De}}T_{\theta\theta} = 0\,, \tag{90}$$

$$\frac{\mathrm{D}}{\mathrm{D}t}\left(\frac{T_{zz}}{F} + \alpha[(Z_{,z})^2 + \varepsilon^2(Z_{,r})^2]\right) + \frac{1}{\mathrm{De}}T_{zz} = 0\,, \tag{91}$$

while F depends essentially only upon s_{rr}, being given by $F \approx 1 + 3b^{-1} + (\varepsilon^2\alpha)^{-1}s_{rr}$. The connection between $s_{rr}, s_{rz}, \tau_{\theta\theta}, \tau_{zz}$ and $S_{rr}, S_{rz}, T_{\theta\theta}, T_{zz}$ is given by

$$\begin{pmatrix} s_{rr} & s_{rz} \\ s_{rz} & \tau_{zz} \end{pmatrix} = c^2 \begin{pmatrix} Z_{,z} & -R_{,z} \\ -Z_{,r} & R_{,r} \end{pmatrix} \begin{pmatrix} S_{rr} & S_{rz} \\ S_{rz} & T_{zz} \end{pmatrix} \begin{pmatrix} Z_{,z} & -Z_{,r} \\ -R_{,z} & R_{,r} \end{pmatrix}, \qquad \tau_{\theta\theta} = c^{-2}T_{\theta\theta}\,. \tag{92}$$

With the approximations $S_{rr} \approx -\alpha F(R_{,z})^2$, $S_{rz} \approx -\alpha F Z_{,z}R_{,z}$, $T_{\theta\theta} \approx \alpha F(\mathrm{e}^{-\mu} - c^2)$ and $T_{zz} \approx \alpha F[\mathrm{e}^{-\mu} - (Z_{,z})^2]$ in which the integrating factor μ for (84) is defined by $\mathrm{D}\mu/\mathrm{D}t = F/\mathrm{De}$, all the contributions $s_{rr}, s_{rz}, \tau_{\theta\theta}$ and τ_{zz} may be approximated by

$$s_{rr} \approx \alpha F(RR_{,z}/r)^2\mathrm{e}^{-\mu}\,, \tag{93}$$

$$s_{rz} \approx -\alpha F R_{,z}(2Z_{,z} + \mathrm{e}^{-\mu}RR_{,r}/r)R/r\,, \qquad \tau_{\theta\theta} \approx \alpha F(r^2\mathrm{e}^{-\mu}/R^2 - 1)\,, \tag{94}$$

$$\tau_{zz} \approx \alpha F\{(RR_{,r}/r)^2\mathrm{e}^{-\mu} - 1\}\,. \tag{95}$$

Inserting these into equation $(87)_1$, together with expression (76) for u, yields together with the relation $R(R_{,r}Z_z - R_{,z}Z_{,r}) = r$ a pair of equations for $R(r,z,t)$ and $Z(r,z,t)$ to be solved with suitable boundary conditions, such as $R = r$ and $Z = 0$ at a rigid plane $Z = 0$. It is clear that the history of deformations is dominated (at least for times such that $t = \mathrm{O}(\mathrm{De})$) by a slowly relaxing form of elasticity, rather than by Newtonian viscous flow. The thin layer approximation yields some simplification to the stress analysis, but it is as yet unclear that the resulting system may be analysed much further analytically.

However, since $\beta = 2 \times 10^{-3}$ the parameter $\nu = \beta\mathrm{De}$ is small for $\mathrm{De} \ll 50$, which reduces $(87)_1$ to an equilibrium equation (slightly modified by the time-relaxation $\mathrm{e}^{-\mu}$, which depends upon material coordinates R, Z as well as upon t.).

B Data values used

Some of the values initially given by Unilever for these quantities were changed substantially during the Study Group week: the values listed here should probably not be regarded as definitive without further checks. Note also that some of the experiments presented by Unilever were not for the AFM but for a different piece of equipment, the "texture analyser", which does the same sort of thing and produces the same sort of force-separation curves, but has quite different parameter values.

Mechanical parameters:

R	radius of sphere, $10\,\mu$m
k	spring constant of cantilever, $0.7\,$N/m
V	retraction velocity in experiment, $360\,$nm/s

Rheological parameters in FENE-P model of saliva:

b	50
η_s	$1.5 \times 10^{-3}\,$Pa s
η_p	$0.68\,$Pa s
λ	$252\,$s

Electrostatic data supplied:

potential of bare glass, $-40\,\mathrm{mV}$
potential of glass coated with polyelectrolyte, $-7\,\mathrm{mV}$
potential of glass coated with chitosan, $+15\,\mathrm{mV}$
thickness of adsorbed layer on substrate, $4\,\mathrm{nm}$
thickness of adsorbed layer on sphere, $50\,\mathrm{nm}$
concentration of coating solution, $250\,\mathrm{g/l}$
mass deposited, $10^{-4}\,\mathrm{mg/cm^2}$

References

[1] Attard P., "Interaction and deformation of viscoelastic particles. Nonadhesive particles", Physical Review E., 2001a, V.63, 061604

[2] Attard P., "Interaction and deformation of viscoelastic particles. 2. Adhesive Particles", Langmuir, 2001b, 17, 4322–4328

[3] Barnocky, G. & Davis, R. H. 1988 Elastohydrodynamic collision and rebound of spheres: experimental verification. Phys. Fluids **31**, 1324–1329.

[4] Bazilevsky, A. V., V. M. Entov, and A. N. Rozhkov, "Liquid filament microrheometer and some of its applications," in *Third European Rheology Conference*, edited by D R. Oliver, Elsevier, New York, (1990), pp. 41–43.

[5] Davis, R. H., Serayssol, J. M. & Hinch, E. J. 1986 The elastohydrodynamic collision of two spheres. J. Fluid Mech. **163**, 479–497.

[6] Derjaguin, B. V., Muller, V. M., Toporov, Y. P. 1975. Effect of contact deformation on the adhesion of particles. J Colloid Interface Sci. 53:314–326.

[7] Entov, V. M. and E. J. Hinch, "Effect of a spectrum of relaxation times on the capillary thinning of a filament of elastic liquid," J. Non-Newtonian Fluid Mech. **72**, 31–54 (1997).

[8] Gaudet S., McKinley G.H., Extensional deformation of non-Newtonian liquid bridges, Computational mechanics, 1998, 21, 461–476

[9] Gondret, P., Lance, M. & Petit, L. 2002 Bouncing motion of spherical particles in fluids. Phys. Fluids **14**, 643–652.

[10] Johnson, K. L., Kendall, K, Roberts, A. D. 1971. Surface energy and the contact of elastic solids. Proc R Soc. London A., 324:301–313.

[11] Joseph, G. G, R. Zenit, M.L. Hunt, A.M. Rosenwinkel, J. Fluid Mech. 433(2001) 329.

[12] Lian, G., M.J. Adams, C. Thornton, J. Fluid Mech. 311 (1996) 141.

[13] Lian G, Xu Y, Huang W, Adams M. J. 2001. On the squeeze flow of a power-law fluid between rigid spheres. JOURNAL OF NON-NEWTONIAN FLUID MECHANICS. 100: 151–164.

[14] Matta, J. E. and R. P. Tytus, "Liquid stretching using a falling cylinder," J. Non-Newtonian Fluid Mech. **35**, 215–229 (1990).

[15] Matar, O.K., Spelt, P.D.M., Stepanek, F. 2006 Collisions of liquid coated solid spherical particles in a viscous fluid. J Colloid Interface Sci. 301:594–606

[16] Maugis, D. 1992. Adhesion of spheres: The JKR-DMT transition using a Dugdale model. J Colloid Interface Sci. 150:243–269.

[17] McKinley G.H., Tripathi A., How to extract the Newtonian viscosity from capillary breakup measurements in a filament rheometer, Journal of Rheology, 2000

[18] Lord Rayleigh, "On the instability of jets," Proc. London Math. Soc. **10**, 4–13 (1878).

[19] Sridhar, T., V. Tirtaatmadja, D. A. Nguyen, and R. K. Gupta, "Measurement of extensional viscosity of polymer solutions," J. Non-Newtonian Fluid Mech. **40**, 271–280 (1991).

[20] Yang, S.-M., L.G. Leal, Y.-S. Kim, J. Colloid Interface Sci. 250 (2002) 457.

[21] Yao M., McKinley G.H., Debbaut B., Extensional deformation, stress relaxation and necking failure of viscoelastic filaments, J. Non-Newtonian Fluid Mechanics, 1998, 79,469–501

[22] Zhang, J. P., Fan, L. S., Zhu, C., Pfeffer, R. & Qi, D. W. 1999 Dynamic behavior of collision of elastic spheres in viscous fluids. Powder Tech. **106**, 98–109.